
ExPLoRA: Parameter-Efficient Extended Pre-Training to Adapt Vision Transformers under Domain Shifts

Samar Khanna^{1*}Medhanie Irgau¹David B. Lobell¹Stefano Ermon^{1,2}¹Stanford University, ²CZ Biohub^{*}Correspondence to: samarkhanna [at] cs.stanford.edu

Abstract

Parameter-efficient fine-tuning (PEFT) techniques such as low-rank adaptation (LoRA) can effectively adapt large pre-trained foundation models to downstream tasks using only a small fraction (0.1%-10%) of the original trainable weights. An under-explored question of PEFT is in extending the pre-training phase without supervised labels; that is, can we adapt a pre-trained foundation model to a new domain via efficient self-supervised pre-training on this new domain? In this work, we introduce ExPLoRA, a highly effective technique to improve transfer learning of pre-trained vision transformers (ViTs) under domain shifts. Initializing a ViT with pre-trained weights on large, natural-image datasets such as from DinoV2 or MAE, ExPLoRA continues the unsupervised pre-training objective on a new domain. In this extended pre-training phase, ExPLoRA only unfreezes 1-2 pre-trained ViT blocks and all normalization layers, and then tunes all other layers with LoRA. Finally, we fine-tune the resulting model only with LoRA on this new domain for supervised learning. Our experiments demonstrate state-of-the-art results on satellite imagery, even outperforming fully pre-training and fine-tuning ViTs. Using the DinoV2 training objective, we demonstrate up to 7% improvement in linear probing top-1 accuracy on downstream tasks while using <10% of the number of parameters that are used in prior fully-tuned state-of-the art approaches. Our ablation studies confirm the efficacy of our approach over other baselines, including PEFT and simply unfreezing more transformer blocks.

1 Introduction

Pre-training foundation models[1] for natural language [2–5] and natural images [6–13] has historically been computationally intensive, often limited to organizations with substantial resources. However, recent advancements in parameter-efficient fine-tuning (PEFT) techniques including low-rank adaptation (LoRA) and others [14–19] have sparked significant interest. These methods aim to adapt foundation models to downstream supervised-learning tasks using a small fraction (0.1%-10%) of the model’s trainable weights, based on the hypothesis that the required weight updates to the pre-trained model have a “low intrinsic rank” [14, 20, 21], or that efficient updates can be achieved by exploiting matrix structure [15, 16].

In this paper, we focus on vision foundation models such as MAE or DinoV2 [7, 6], which are trained on large-scale natural-image datasets and exhibit robust generalization capabilities measured via linear probing or KNN classification for downstream tasks. Despite the large investments in developing such models for natural images, they underperform when applied to other domains with visual data (e.g., medical or remote sensing images). For example, fine-tuning a model pre-trained on natural images on satellite image classification tasks is not as effective as fine-tuning models that were pre-trained on satellite images [22, 23]. To bridge this gap, prevailing approaches invest

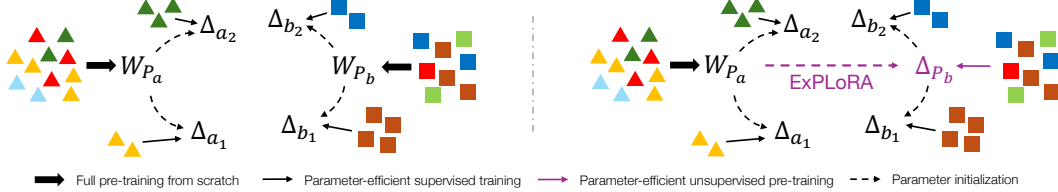


Figure 1: Consider two (fairly different) image domains, a and b . **Left:** the traditional paradigm of pre-training from scratch on each different domain to yield W_{P_a} and W_{P_b} , and then fine-tuning on the target datasets i to yield Δ_{a_i} , Δ_{b_i} , for domains a and b , respectively. **Right:** our approach, which is to initialize with pre-trained weights from domain a and then learn unsupervised weights Δ_{P_b} for domain b in a parameter-efficient manner.

similarly large levels of compute to pre-train foundation models on the new domains, inspired by techniques developed for natural images[22–27].

In this work, we challenge this paradigm (fig. 1), asking whether pre-training from scratch on each new domain is strictly necessary, since doing so is expensive (in compute and time) and precludes knowledge transfer from natural images. Instead, we wish to more efficiently and effectively leverage the large amount of semantic information encoded in natural-image vision foundation models to adapt them to new domains. Our proposed solution addresses these concerns using PEFT techniques for domain adaptation via self-supervised learning.

We introduce ExPLoRA, which generalizes vision foundation models to new domains by extending the pre-training phase with parameter-efficient techniques. We initialize a vision transformer (ViT)[28] with pre-trained weights from large, natural-image datasets (such as MAE or DinoV2). Selectively unfreezing the last, or the first and last transformer blocks, we tune remaining weights with LoRA and continue unsupervised pre-training on the new domain. Subsequently fine-tuning using linear probing or LoRA on this new domain for supervised learning outperforms prior state-of-the-art (SoTA) approaches while training less than 5%-10% of the original weights. On satellite imagery, for example, we demonstrate more than 7% improvement in linear probing top-1 accuracy, and even an improvement over prior SoTA fully pre-trained and fine-tuned techniques. We conduct an extensive study on RGB, temporal, and multi-spectral satellite images, either matching or outperforming prior methods that use full-rank pre-training from scratch. Our ablation studies confirm the superiority of our approach over alternatives. We also demonstrate generalization to different domains, such as wildlife imagery and medical images on the WILDS[29] benchmark. Our contributions include:

1. Introducing ExPLoRA, a novel parameter-efficient method that extends unsupervised pre-training on target domains, achieving state-of-the-art supervised-learning performance using a fraction of the original ViT weights.
2. Conducting a comprehensive case study on satellite imagery, showcasing improvements in linear probing top-1 accuracy and outperforming existing techniques on datasets like fMoW. We also demonstrate generalization to other domains such as wildlife and medical imagery.

2 Related Work

Visual Foundation Models Visual foundation models(VFMs), such as DinoV2 or masked autoencoders (MAE), have demonstrated remarkable performance across downstream tasks such as classification or semantic segmentation [1, 6, 7]. However, there has also been a rise in domain-specific VFMs [22, 27, 30–32], like SatMAE, which is designed to handle temporal or multi-spectral satellite imagery[22]. With these models containing hundreds of millions of parameters, efficient adaptation to downstream tasks has become a key research focus.

PEFT PEFT methods have gained widespread adoption for efficiently adapting large models to various downstream tasks, mitigating the prohibitive costs associated with full model tuning by updating only a fraction of the parameters. For example, LoRA learns low-rank weight updates to frozen weights, while other methods modify the frequency or number of trainable parameters per layer [14, 17–19, 33]. Lialin et al. [19] introduce LoRA for pre-training via the sum of multiple low-rank matrices, but require full parameter tuning as a “warm start”. Some approaches use multiplicative orthogonal weight updates to frozen weights, effectively retaining pre-training knowledge

[16, 15]. While our ExPLoRA method can be configured with LoRA fine-tuning for downstream tasks, it supplements existing PEFT methods rather than replacing them, particularly in the case of unsupervised domain adaptation.

Domain Adaptation The central problem in domain adaptation is managing the distribution shift with respect to training and testing data. Domain adaptation approaches have explored this issue from several perspectives[34]. Discrepancy-based methods minimize the difference between feature distributions of the source and target domains using discrepancy metrics[35–37] for domain loss. Adversarial methods aim to amplify domain confusion while simultaneously being rigorously trained to recognize and distinguish between different domains [38–40]. Group DRO aims to minimize the loss in the worst-case domain within the context of domain adaptation, specifically addressing subpopulation shift, where data distributions differ but may have some overlap [41, 42].

3 Background

MAE The masked-autoencoder (MAE) [7] is an effective self-supervised learning technique for ViTs. It utilizes an asymmetrical encoder-decoder architecture on images $\mathbf{x} \in \mathbb{R}^{C \times H \times W}$ (height, width, channels H, W, C), where patches are masked before being processed by the ViT encoder \mathcal{L} . The visible embedded patches are then reconstructed using a smaller ViT decoder \mathcal{L}_D , with the training objective being a mean-squared error loss on the visible pixels. MAE has been widely adopted in various domains including satellite imagery [22], video [43], and other modalities[44, 45]. However, pre-training ViTs as MAEs typically requires subsequent full fine-tuning for downstream tasks, making them computationally intensive.

DinoV2 DinoV2 [6] is a robust self-supervised learning technique for ViTs. Unlike MAE, DinoV2 features have demonstrated strong zero-shot performance, enabling adaptation to downstream tasks even with a frozen ViT backbone. During pre-training, DinoV2 maintains two copies of a ViT encoder: the student (trainable) and the teacher, which is updated using an exponential-moving average of the student’s parameters. The training objective incorporates a global, image-level loss from Dino [11] and a patch-based loss from iBOT [8]. Various techniques including KoLeo regularization [46] and Sinkhorn-Knopp centering [10] are utilized, as described in [6].

LoRA Low-rank adaptation (LoRA) [14] assumes that the weight update to change a set of unsupervised pre-trained weights to supervised fine-tuned weights lives in a low-rank subspace,

$$W \approx W_0 + \Delta_W = W + BA \quad (1)$$

where $W \in \mathbb{R}^{k_2 \times k_1}$ are the final, task-specific fine-tuned weights, $W_0 \in \mathbb{R}^{k_2 \times k_1}$ are the pre-trained weights, $\Delta_W \in \mathbb{R}^{k_2 \times k_1}$ is the weight update required to translate the pre-trained weights W_0 to the fine-tuned weights W . The key is that $\Delta_W = BA$ where $B \in \mathbb{R}^{k_2 \times r}$ and $A \in \mathbb{R}^{r \times k_1}$. That is, A and B form a low-rank factorization of Δ_W , where the rank $r \ll \min(k_1, k_2)$.

4 Problem Setup

Consider a set of image domains $\mathcal{D} = \{1, 2, \dots\}$ and an associated data distribution for each domain $p_d(\mathbf{x})$, where $d \in \mathcal{D}$ and images $\mathbf{x} \in \mathbb{R}^{C_d \times H_d \times W_d}$. Here C_d , H_d and W_d represent the channel, height and width dimensions of images of each domain, respectively. Let $D_P, D_F \subset \mathcal{D}$ be a set of domains representing the pre-training and fine-tuning data distributions $p_{D_P}(\mathbf{x})$ (eg: internet-scale natural image data) and $p_{D_F}(\mathbf{x})$ (eg: satellite data), respectively. Next, the fine-tuning joint distributions for each domain $d_F \in D_F$ are $p_{d_F}(\mathbf{x}, \mathbf{y})$, where \mathbf{y} is the supervised-learning label.

We then assume access to the following: (i) pre-trained weights W_{D_P} , indexed by the collection of pre-training domains D_P , which have already been obtained via unsupervised learning (ii) samples from $p_{D_F}(\mathbf{x})$ representing unlabeled images from a new, different domain D_F (iii) a collection of target datasets $d_F \in D_F$ from the new domain D_F , sampled from distributions $p_{d_F}(\mathbf{x}, \mathbf{y})$. Thus, we would like to learn optimal weights W_{d_F} in a parameter-efficient manner for each supervised-learning dataset while leveraging knowledge stored in W_{D_P} .

LoRA solves this in the following way:

$$W_{d_F} \approx W_{D_P} + \Delta_{d_F} = W_{D_P} + B_{d_F} A_{d_F} \quad (2)$$

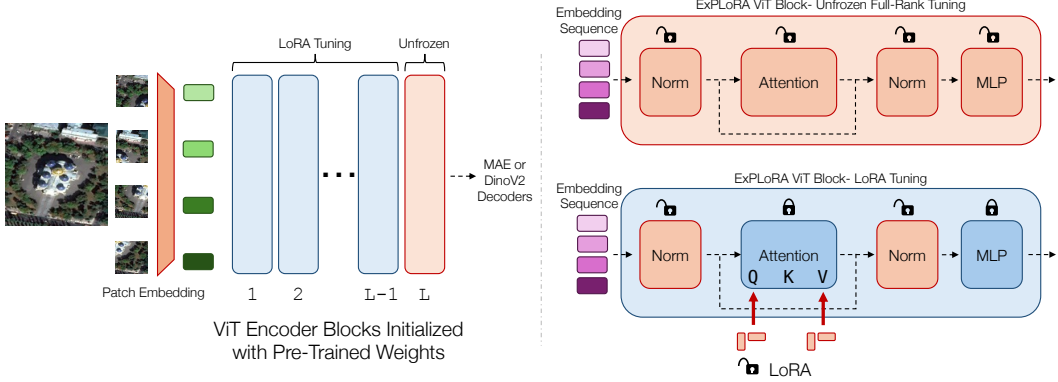


Figure 2: An overview of ExPLoRA. The set \mathcal{L} of L ViT blocks is partitioned into two sets: \mathcal{U} , which denotes blocks whose parameters are completely unfrozen, and $\mathcal{L} \setminus \mathcal{U}$ which denotes blocks that undergo LoRA tuning (only on the Q , V attention matrices). Note that the normalization layers are always unfrozen across all blocks.

The LoRA hypothesis is that the update Δ_{d_F} resides in a low-rank subspace when adapting pre-trained weights W_{D_P} to fine-tuned weights W_{d_F} . This hypothesis empirically seems to work when pre-training and fine-tuning distributions are similar, or where $d_F \in D_P$. However, we empirically find that when adapting to a significantly different domain, where D_F has little to no overlap with D_P (eg: natural images to multi-spectral satellite data), this hypothesis fails to hold (see section 6.1.3).

To address this challenge, the traditional solution (fig. 1) has been to begin pre-training from scratch on the new domains of interest D_F , and then use PEFT for each dataset d_F , representing the following:

$$W_{d_F} \approx W_{D_F} + \Delta_{d_F} \quad (3)$$

where W_{D_F} now represent unsupervised pre-trained weights learned from the data distribution $p_{D_F}(\mathbf{x})$. However, this is wasteful: learning W_{D_F} from scratch can require prohibitively large amounts of additional compute to complete full-rank pre-training for each new domain of interest.

Our goal is thus the following: can we still leverage the rich semantic information encoded in W_{D_P} and learn W_{D_F} for a new domain in a parameter-efficient manner? Concretely, we would like to factorize W_{d_F} as follows:

$$W_{d_F} \approx W_{D_P} + \Delta_{D_F} + \Delta_{d_F} \quad (4)$$

where $\Delta_{D_F} \in \mathbb{R}^{k_2 \times k_1}$ is an additional update matrix learned for the collection of fine-tuning domains D_F . Our key requirements for Δ_{D_F} are: (i) Δ_{D_F} must be learned via unsupervised pre-training on $p_{D_F}(\mathbf{x})$ (ii) Δ_{D_F} must only require learning a fraction of the $k_1 k_2$ parameters that form W_{D_P}

Note that successfully learning Δ_{D_F} , would obviate the vast computing resources that are otherwise necessary to fully train foundation models for the new domain. Importantly, we emphasize learning Δ_{D_F} in an *unsupervised* manner so that the resulting model $W'_{D_F} = W_{D_P} + \Delta_{D_F} \approx W_{D_F}$ retains the benefits of pre-trained foundation models, such as feature extraction, effective linear-probing, and generalization to further downstream tasks.

5 Method

To learn Δ_{D_F} , we propose ExPLoRA (i.e. **E**xtended **P**re-training with **L****O****R****A**). Let $\mathcal{L} = \{1, \dots, L\}$ denote the set of all L ViT blocks (or layers). For ViT-Large (ViT-L), $\mathcal{L} = \{1, \dots, 24\}$. The ExPLoRA approach is as follows:

- (i) Initialize the ViT with W_{D_P} from a large pre-training dataset (eg: DinoV2 or MAE weights).
- (ii) Unfreeze all parameters of a subset of blocks $\mathcal{U} \subset \mathcal{L}$. Typically, $\mathcal{U} = \{L\}$ or $\mathcal{U} = \{1, L\}$.
- (iii) For all other blocks $\mathcal{L} \setminus \mathcal{U}$, freeze all parameters and use LoRA with rank r on the Q and V weights of the attention layer. Also unfreeze the normalization layers of these blocks.
- (iv) Train the resulting model on *unlabeled* images $\mathbf{x} \sim p_{D_F}(\cdot)$ of the new domain D_F , with the same unsupervised objective as what was used for W_{D_P} (eg: DinoV2 or MAE training objective).

In terms of notation, D-ExPLoRA-[L]-r32 would then denote a ViT initialized with DinoV2 weights (as opposed to M, which is MAE weights), where $\mathcal{U} = \{L\}$, and LoRA rank 32 is used on the Q, V matrices of every attention layer in $\mathcal{L} \setminus \mathcal{U}$. In this way, Δ_{D_F} requires 5-10% of the original parameters of the ViT, and we show it learns unsupervised representations for Δ_{D_F} that can match or even outperform learning W_{D_F} directly from scratch, through full pre-training.

ExPLoRA for DinoV2 For our experiments, we use the DinoV2 ViT-L model as W_{D_P} , without registers [47]. We unfreeze the 24th block of the ViT, and use LoRA only on the query Q and value V matrices of each attention layer in all other blocks. We also unfreeze the normalization layers (which require very few parameters) throughout the network. We train each of the Dino, iBOT, and Koleo linear heads fully, without any frozen parameters.

ExPLoRA for MAE We initialize both the MAE encoder and decoder with pre-trained weights. We only unfreeze the last block of the ViT encoder, and tune the Q, V matrices of each attention layer in all other blocks (including all blocks of the decoder) with LoRA.

For the multi-spectral MAE introduced in [22] we need to unfreeze the patch embedding layers for each group of channels (as these cannot be initialized from W_{D_P} since W_{D_P} only considers 3 channel RGB inputs). We then find that when using ExPLoRA, unfreezing blocks 1 and L is necessary to successfully achieve domain transfer.

Fine-tuning While fine-tuning DinoV2, we discard the linear heads used for the pre-training loss components (section 3), and load all other model weights. Similarly, for MAE, we discard the decoder weights. We then initialize a linear head for classification, or decoder for segmentation, either of which is fully trainable. Freezing all ViT encoder weights, we then use LoRA-r8 on the Q, V matrices of every attention layer. We find that the drop-path augmentation [48] is especially useful for fine-tuning, and use a value of 0.2 for the ViT-L models.

6 Experiments

Our experimental results first consist of a case study on satellite imagery (section 6.1), including an ablation study in section 6.1.2. We then further evaluate on downstream tasks in sections 6.1.3, 6.1.4 and 6.2. Training details including hyperparameter and compute configurations are mentioned in appendix B. Our results achieve a new SoTA top 1 accuracy of 79.1% ($\uparrow 1.3\%$) on the competitive fMoW-RGB benchmark, outperforming fully pre-trained and fine-tuned models while using 6% of the ViT encoder parameters. We also achieve a $\uparrow 7.3\%$ improvement in linear probing accuracy on the same dataset. Across other satellite datasets, we match fully-pretrained prior state-of-the-art methods, and demonstrate competitive performance on WiLDS benchmark datasets as well.

6.1 Case Study: Satellite Imagery

We begin by examining satellite images largely because of the proliferation in works developing foundational models for satellite imagery via pre-training from scratch[22–25] and since they represent a significant domain shift from natural images. We thus structure our study in a few parts: (i) Evaluating ExPLoRA on RGB satellite images, both for linear probing and PEFT fine-tuning (ii) Demonstrating ExPLoRA ability to handle a domain shift from natural images to multi-spectral and temporal satellite inputs, a more difficult translation. (iii) Evaluating models pre-trained with ExPLoRA on downstream satellite datasets.

6.1.1 RGB Satellite Images

Dataset We first consider the functional map of the world (fMoW) dataset of high-resolution satellite images, each paired with one of 62 classification labels [49]. This dataset is used as a benchmark for multiple satellite-image foundation models [22–24].

We compare our results in table 1 against both prior fully pre-trained SoTA foundation models as well as PEFT techniques applied on ViTs pre-trained with MAE and/or DinoV2 weights. Our results demonstrate that D-ExPLoRA-[L]-r64 is SoTA in terms of fMoW-RGB average accuracy at 79.15%. ExPLoRA outperforms techniques that require fully pre-training ViTs on fMoW while using 6% of

| Model | Backbone | PEFT | Pre-train #Params | Fine-tune #Params | Top 1 Acc. |
|-----------------------|----------|-----------|-------------------|-------------------|--------------|
| GASSL [23] | ResNet50 | Full | 23.6M | 23.6M | 71.55 |
| ScaleMAE [24] | ViT-L | Full | 303.3M | 303.3M | 77.80 |
| SatMAE [22] | ViT-L | Full | 303.3M | 303.3M | 77.78 |
| MAE [7] | ViT-L | Full | - | 303.3M | 76.91 |
| SatMAE [22] | ViT-L | LoRA-r8 | 303.3M | 0.8M | 76.10 |
| MAE [7] | ViT-L | LoRA-r8 | - | 0.8M | 76.21 |
| MAE [7] | ViT-L | BOFT-b2m8 | - | 0.9M | 72.40 |
| DinoV2 [6] | ViT-L | LoRA-r8 | - | 0.8M | 78.08 |
| M-ExPLoRA- $[L]$ -r64 | ViT-L | LoRA-r8 | 18.7M | 0.8M | 76.55 |
| D-ExPLoRA- $[L]$ -r64 | ViT-L | LoRA-r8 | 18.7M | 0.8M | 79.15 |

Table 1: Results on the fMoW-RGB validation dataset. The “Pre-train #Params” and “Fine-tune #Params” refer to the trainable parameters of the ViT encoder required on the *new* domain, i.e. satellite images.

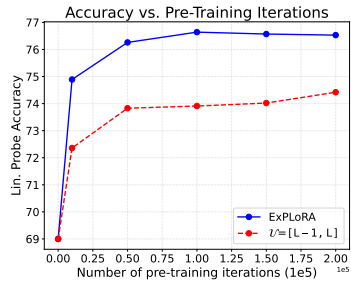


Figure 3: Lin. probe accuracy vs. number of training iterations, demonstrating ExPLoRA’s efficiency even with few pre-training updates.

| Blocks | LoRA Rank | Norm Unfrozen | LoRA Layers | Num. Params | Top 1 Acc. |
|------------|-----------|---------------|-------------|-------------|--------------|
| $[L-1, L]$ | 0 | ✓ | [] | 25.3M | 74.42 |
| [] | 256 | ✓ | [Q, V] | 25.9M | 74.82 |
| [] | 128 | ✓ | A11 | 33.1M | 55.03 |
| [1] | 32 | ✓ | [Q, V] | 15.7M | 73.39 |
| [L] | 32 | ✗ | [Q, V] | 15.6M | 75.14 |
| [L] | 8 | ✓ | [Q, V] | 13.4M | 75.23 |
| [L] | 32 | ✓ | [Q, V] | 15.7M | 75.44 |
| [L] | 64 | ✓ | [Q, V] | 18.7M | 76.53 |

Table 3: Ablation study using DinoV2-ExPLoRA, measuring linear-probing accuracy on fMoW-RGB. If the LoRA rank is > 0 , LoRA is only used on the frozen ViT blocks. All results are obtained by using concatenated features from the last 4 ViT blocks.

the original ViT encoder parameters. We also note that the original LoRA configuration outperforms other PEFT techniques when paired with the drop-path regularization technique. For example, we find that BOFT does not pair well with drop-path, instead performing most effectively with a custom multiplicative dropout technique. We include the result with the best hyperparameter configuration for each row in table 1.

| Method | Backbone | Top 1 Acc. |
|---------------------------------|----------|--------------|
| GASSL [23] | ResNet50 | 68.32 |
| SatMAE [22] | ViT-L | 65.94 |
| ScaleMAE [24] | ViT-B | 67.30 |
| CrossScaleMAE [25] | ViT-B | 69.20 |
| DinoV2 [6] | ViT-L | 67.60 |
| DinoV2 \dagger [6] | ViT-L | 69.00 |
| D-ExPLoRA- $[L]$ -r64 | ViT-L | 75.77 |
| D-ExPLoRA- $[L]$ -r64 \dagger | ViT-L | 76.53 |

Table 2: Linear-probing on fMoW-RGB. The first four rows fully pre-train on the dataset. \dagger denotes concatenating features from the last 4 ViT blocks.

ExPLoRA outperforms domain-specific prior SoTA solutions (rows 1-4), as well as DinoV2, which suggests successful transfer learning on the target domain by leveraging knowledge from pre-training on natural images.

6.1.2 Ablation study

We perform an ablation study (table 3) on linear-probing performance for fMoW-RGB to determine whether our proposed configuration performs optimally. A natural question is whether the improvement in performance stems primarily from unfreezing blocks, or from LoRA-tuning the rest of the ViT. We investigate this by unfreezing blocks $L, L-1$ in the row 1 (with no LoRA), and comparing that with ExPLoRA- L -r8 in row 6. As seen, unfreezing an extra block consumes almost double

the number of parameters, but fails to yield the same improvement in performance. Thus, simply increasing the number of unfrozen blocks will likely improve performance, but will not do so as effectively as ExPLoRA, and will also significantly and sharply decrease the parameter-efficiency. As seen in fig. 3, ExPLoRA also enables faster convergence (blue) with fewer training iterations compared to unfreezing more blocks (red).

Next, we investigate whether high LoRA ranks used on all ViT layers (i.e. all attention and MLP matrices, not just Q, V) is beneficial. Surprisingly, this significantly harms learning (row 3). In fact, it is much less effective than using just LoRA- r -256 on the Q, V matrices of all \mathcal{L} blocks (row 2). However, both rows 2 and 3 are much less parameter-efficient than ExPLoRA (rows 4-6).

The choice of \mathcal{U} matters as well. As seen in row 4 vs the second to last row, for the DinoV2 objective, $\mathcal{U} = [1]$ is not as effective as $\mathcal{U} = [L]$, ceteris paribus. We also notice a slight drop in accuracy from leaving the normalization layers across the ViT frozen, seen in row 5.

Lastly, we investigate the impact of LoRA rank on ExPLoRA. Changing the rank from 8 to 32 has a small improvement, but changing from 32 to 64 brings about a much larger improvement, with only a relatively small increase in trainable parameters. This demonstrates that higher ranks are necessary during pre-training for effective learning on the new domain. One hypothesis for the effectiveness of pairing unfreezing blocks with LoRA tuning is that the low-rank updates to the ViT backbone “nudge” the sequence of embedded visual tokens from D_P to those representing D_F , which then enables the unfrozen ViT block to effectively compress data from the new domain.

6.1.3 Multi-Spectral Satellite Images

Dataset Next, we consider the fMoW-Sentinel dataset, a large dataset of Sentinel-2 images used in [22]. Each image consists of 13 spectral bands and is paired with one of 62 classes.

With fMoW-Sentinel, we aim to assess the feasibility of domain transfer from natural images to multi-spectral, low-resolution satellite images. This presents a significant challenge compared to fMoW-RGB, as none of the natural image datasets in D_P include sensor information beyond visible light RGB bands. We utilize the group-channel ViT-L SatMAE model introduced in [22], initializing it with MAE self-supervised weights from the natural image domain. Since the patch embedding layers differ from those of MAE, we unfreeze and train them from scratch during ExPLoRA pre-training, resulting in minimal overhead to the parameter count.

| Model | Backbone | PEFT | Pre-train #Params | Fine-tune #Params | Top 1 Acc. |
|---------------------|-----------|---------|-------------------|-------------------|--------------|
| ImgNet-Supervised | ResNet152 | Full | 60.3M | 60.3M | 54.46 |
| MAE [7] | ViT-L | Full | - | 303.3M | 51.61 |
| SatMAE [22] | ViT-L | Full | 303.3M | 303.3M | 61.48 |
| MAE [7] | ViT-L | LoRA-r8 | - | 0.8M | 46.97 |
| SatMAE [22] | ViT-L | LoRA-r8 | 303.3M | 0.8M | 59.48 |
| MAE-[1,2,L-1,L] | ViT-L | LoRA-r8 | 51.5M | 0.8M | 54.12 |
| M-ExPLoRA-[L]-r32 | ViT-L | LoRA-r8 | 16.2M | 0.8M | 51.84 |
| M-ExPLoRA-[1,L]-r32 | ViT-L | LoRA-r8 | 29.7M | 0.8M | 60.15 |

Table 4: Results on the fMoW-Sentinel validation set. The “Pre-train #Params” and “Fine-tune #Params” refer to the trainable parameters required on the *new* domain, i.e. multi-spectral satellite images. “MAE-[1,2,L-1,L]” refers to initializing the group-channel SatMAE model with MAE weights, unfreezing blocks 1,2,23,24 for ViT-L, and then continuing pre-training on fMoW-Sentinel.

From table 4, we observe the challenge of domain transfer from natural images to multi-spectral satellite images, as discussed in section 5. Even fully fine-tuning from MAE weights results in nearly a 10% drop in accuracy (row 2). LoRA tuning solely from MAE weights (row 4) performs even worse. Ablating by initializing with MAE weights and unfreezing only 4 transformer blocks during pre-training (row 6) is insufficient to bridge the domain gap. Notably, with ExPLoRA, unfreezing the first and last transformer blocks yields surprisingly good results, surpassing even fully pre-training from scratch (when using LoRA for fine-tuning). This underscores ExPLoRA’s ability to bridge wide domain gaps while utilizing only a fraction (in this case, around a tenth) of the original parameters.

| Method | PEFT | Top 1 Acc. |
|-----------------------|---------|--------------|
| GASSL [23] | Full | 74.11 |
| SatMAE [22] | Full | 79.69 |
| MAE [7] | LoRA-r8 | 69.30 |
| SatMAE [22] | LoRA-r8 | 75.27 |
| M-ExPLoRA- $[L]$ -r32 | LoRA-r8 | 75.98 |

Table 5: fMoW-Temporal validation set results

| Method | PEFT | mIoU |
|-----------------------|------------|--------------|
| GASSL [23] | Full | 78.51 |
| SatMAE [22] | Full | 78.07 |
| ScaleMAE [24] | Full | 78.90 |
| DinoV2 [6] | Lin. Probe | 76.21 |
| DinoV2 [6] | LoRA-r8 | 76.69 |
| D-ExPLoRA- $[L]$ -r64 | LoRA-r8 | 76.69 |

Table 7: SpaceNet validation set results

| Method | PEFT | Top 1 Acc. |
|--------------------------|-----------|--------------|
| SeCo [53] | Full | 93.14 |
| SatMAE [22] | Full | 98.98 |
| SatMAE [22] | LoRA-r8 | 98.73 |
| DinoV2 [6] | BOFT-b8m2 | 96.60 |
| M-ExPLoRA- $[1, L]$ -r32 | LoRA-r8 | 98.54 |

Table 6: EuroSAT validation set results

| Method | PEFT | Top 1 Acc. |
|-----------------------|------------|--------------|
| SatMAE [22] | Full | 94.80 |
| ScaleMAE [24] | Full | 95.70 |
| GASSL [23] | Lin. Probe | 89.94 |
| SatMAE [22] | Lin. Probe | 88.30 |
| ScaleMAE [24] | Lin. Probe | 89.60 |
| DinoV2 [6] | Lin. Probe | 96.34 |
| D-ExPLoRA- $[L]$ -r64 | Lin. Probe | 97.16 |

Table 8: Resisc-45 validation set results

6.1.4 Additional Satellite Datasets

fMoW-Temporal Also sourced from fMoW-RGB [49], each input is a sequence of up to 3 images of the same location, distributed temporally, and paired with one of 62 classes. Since the inputs are now temporal sequences, we initialize the temporal MAE architecture from [22] with MAE weights, and pre-train on the dataset’s training images (without labels) with $\mathcal{U} = [L]$ and LoRA rank 32. Our LoRA-tuned model then outperforms the domain-specific SatMAE for PEFT (table 5), demonstrating successful transfer learning at a fraction of the pre-training parameters used by temporal SatMAE, which was fully pre-trained and fully fine-tuned on this dataset.

EuroSAT The dataset contains 27,000 13-band satellite images of 10 classes [50], sourced from Sentinel-2. For ExPLoRA, we don’t pre-train on the training set of this dataset, and instead use LoRA fine-tuning starting with the pre-trained weights learned in row 8 of table 4. We demonstrate improved performance over DinoV2, and match the performance achieved by the domain-specific SatMAE which was fully pre-trained on fMoW-Sentinel, and fully fine-tuned on EuroSAT (table 6). This demonstrates the successful use of our extended pre-trained model on further downstream datasets.

SpaceNet-v1 This dataset contains high resolution satellite images, each paired with a segmentation mask for buildings [51]. The training and test sets consist of 5000 and 1940 images, respectively. For ExPLoRA, we pre-train on the training set. A significant portion of the data consists of images with extensive black regions, indicating areas without meaningful visual information. Considering this limitation and the small dataset size, it is not clear whether additional pretraining is effective. We find that, despite this, ExPLoRA remains on par with the LoRA tuned DinoV2 model and remains competitive with the fully pre-trained and fully fine-tuned domain-specific models (table 7).

RESISC-45 The benchmark RESISC-45 [52] dataset consists of 31,500 satellite images of varying resolution (0.2m-30m GSD), with 45 classes. The data is split into 25,200 training and 6,300 validation images, as per Reed et al. [24]. In table 8, our D-ExPLoRA pre-trained on only high-resolution fMoW-RGB images achieves SoTA results of 97.16% on multi-resolution RESISC-45 images, with just linear-probing. Since we use the same pre-trained model as in the last row of table 1, we demonstrate successful transfer learning from ExPLoRA pre-training, without requiring any additional modifications for scale-aware representation learning [24].

6.2 WiLDS Datasets

We also test ExPLoRA on the WiLDS [29] benchmark, specifically the Camelyon17 [54] and iWildcam [55] datasets, representing domain transfers to medical imagery and wildlife imagery, respectively. Note that the jump from natural images to medical images is larger than for wildlife images, likely because natural image datasets such as ImageNet[56] already contain many images of animals. However, there are little to no medical images such as images of cell tissue in the pre-training datasets for natural image models.

| Method | PEFT | Top 1 Acc. |
|-------------------|------------|--------------|
| ConnectLater[57] | Full | 93.90 |
| ICON | Full | 90.10 |
| DinoV2 [6] | Lin. Probe | 93.27 |
| DinoV2 [6] | LoRA-r8 | 92.97 |
| D-ExPLoRA-[L]-r32 | Lin. Probe | 94.41 |
| D-ExPLoRA-[L]-r32 | LoRA-r8 | 94.21 |

Table 9: Results on the validation set of Camelyon17

| Method | PEFT | Top 1 Acc. |
|-------------------|------------|--------------|
| DinoV2 [6] | Lin. Probe | 66.04 |
| DinoV2 [6] | LoRA-r8 | 67.10 |
| D-ExPLoRA-[L]-r32 | Lin. Probe | 62.95 |
| D-ExPLoRA-[L]-r32 | LoRA-r8 | 68.07 |

Table 10: Results on the validation set of iWildcam

Camelyon17 The WILDS Camelyon17 dataset consists of images of cancerous and non-cancerous cell tissue organized in labeled and unlabeled splits. We use the “train-unlabeled” split for pre-training ExPLoRA, and either use LoRA fine-tuning or linear probing on the training set of the labeled split. We report accuracy on the binary classification problem and compare with entries on the WILDS leaderboard which use unlabeled data. Our results in table 9 demonstrate improved performance over domain-specific methods as well as DinoV2, once again successfully bridging the domain gap.

iWildcam The iWildcam classification requires identifying one of 182 animal species given an image. We pre-train on the training set of the iWildcam classification task, finding that this outperforms pre-training on the extra-unlabeled set. In table 10, we find an improvement over DinoV2 using LoRA-r8 PEFT. Surprisingly, the linear probing performance of the ExPLoRA suffers in comparison with DinoV2, suggesting possible loss in knowledge-transfer due to a small domain gap.

7 Conclusion and Discussion

In this paper, we introduce ExPLoRA, a novel pre-training strategy to adapt pre-trained ViT foundation models for natural images to additional visual domains such as satellite imagery or medical data. We challenge the common paradigm of expensive pre-training from scratch for each new visual domain by offering a solution to transfer knowledge from foundation models that is both parameter-efficient and effective (even outperforming domain-specific foundation models). Our hope is that ExPLoRA enables further use of foundation models on domains other than natural images without requiring vast computational resources for pre-training.

While effective, there are many aspects of ExPLoRA that deserve further study. The strategy of unfreezing a small number of blocks combines extremely well with PEFT techniques such as LoRA—we hope that future work investigates the reason behind this in further detail. Unresolved questions also include whether other parameter-efficient techniques might be better suited to work with ExPLoRA during pre-training. Further work to evaluate ExPLoRA for natural language domains would be valuable, as would an investigation into whether we can do away entirely with unfreezing a transformer block.

Broader Impact

As the scale of models and datasets grows exponentially, access to the computing power necessary to develop and make use of foundation models is increasingly restricted to the hands of a few organizations. Many researchers in academia or smaller companies are then completely dependent on the resources of such organizations in order to leverage ML for their own research or use-cases. Techniques such as PEFT can alleviate this dependence and enable those with much fewer computational resources to perform investigations and customize models for their own use-cases. We hope that ExPLoRA further enables ML practitioners and users to tailor foundation models for their own needs while requiring comparatively few resources. Our hope in doing so is to accelerate the deployment and use of ML for important domains such as sustainability or medicine.

For satellite images, for example, automated analyses that accurately characterize activity on the planet can guide an array of social, economic and environmental policies. Manually curating such observations is time-consuming and expensive, but pre-training foundation models on such data carries its own costs and environmental impact (see appendix C). Thus, we provide a cheaper and more effective way to distill knowledge from foundation models that were already trained on natural images. Insights gained from such a model can further aid researchers and policymakers at a fraction of the cost, enabling more flexible uses of foundation models towards downstream datasets and tasks.

Acknowledgements

This research is based upon work supported in part by the Office of the Director of National Intelligence (ODNI), Intelligence Advanced Research Projects Activity (IARPA), via 2021-2011000004, NSF(#1651565), ARO (W911NF-21-1-0125), ONR (N00014-23-1-2159), CZ Biohub, HAI. The views and conclusions contained herein are those of the authors and should not be interpreted as necessarily representing the official policies, either expressed or implied, of ODNI, IARPA, or the U.S. Government. The U.S. Government is authorized to reproduce and distribute reprints for governmental purposes notwithstanding any copyright annotation therein.

References

- [1] Rishi Bommasani, Drew A Hudson, Ehsan Adeli, Russ Altman, Simran Arora, Sydney von Arx, Michael S Bernstein, Jeannette Bohg, Antoine Bosselut, Emma Brunskill, et al. On the opportunities and risks of foundation models. *arXiv preprint arXiv:2108.07258*, 2021.
- [2] Tom Brown, Benjamin Mann, Nick Ryder, Melanie Subbiah, Jared D Kaplan, Prafulla Dhariwal, Arvind Neelakantan, Pranav Shyam, Girish Sastry, Amanda Askell, et al. Language models are few-shot learners. *Advances in neural information processing systems*, 33:1877–1901, 2020.
- [3] Aakanksha Chowdhery, Sharan Narang, Jacob Devlin, Maarten Bosma, Gaurav Mishra, Adam Roberts, Paul Barham, Hyung Won Chung, Charles Sutton, Sebastian Gehrmann, et al. Palm: Scaling language modeling with pathways. *Journal of Machine Learning Research*, 24(240):1–113, 2023.
- [4] Hugo Touvron, Thibaut Lavril, Gautier Izacard, Xavier Martinet, Marie-Anne Lachaux, Timothée Lacroix, Baptiste Rozière, Naman Goyal, Eric Hambo, Faisal Azhar, et al. Llama: Open and efficient foundation language models. *arXiv preprint arXiv:2302.13971*, 2023.
- [5] Albert Q Jiang, Alexandre Sablayrolles, Antoine Roux, Arthur Mensch, Blanche Savary, Chris Bamford, Devendra Singh Chaplot, Diego de las Casas, Emma Bou Hanna, Florian Bressand, et al. Mixtral of experts. *arXiv preprint arXiv:2401.04088*, 2024.
- [6] Maxime Oquab, Timothée Darcet, Théo Moutakanni, Huy Vo, Marc Szafraniec, Vasil Khalidov, Pierre Fernandez, Daniel Haziza, Francisco Massa, Alaeldin El-Nouby, et al. Dinov2: Learning robust visual features without supervision. *arXiv preprint arXiv:2304.07193*, 2023.
- [7] Kaiming He, Xinlei Chen, Saining Xie, Yanghao Li, Piotr Dollár, and Ross Girshick. Masked autoencoders are scalable vision learners. In *Proceedings of the IEEE/CVF conference on computer vision and pattern recognition*, pages 16000–16009, 2022.
- [8] Jinghao Zhou, Chen Wei, Huiyu Wang, Wei Shen, Cihang Xie, Alan Yuille, and Tao Kong. ibot: Image bert pre-training with online tokenizer. *arXiv preprint arXiv:2111.07832*, 2021.
- [9] Xinlei Chen, Haoqi Fan, Ross Girshick, and Kaiming He. Improved baselines with momentum contrastive learning. *arXiv preprint arXiv:2003.04297*, 2020.
- [10] Mathilde Caron, Ishan Misra, Julien Mairal, Priya Goyal, Piotr Bojanowski, and Armand Joulin. Unsupervised learning of visual features by contrasting cluster assignments. *Advances in neural information processing systems*, 33:9912–9924, 2020.
- [11] Mathilde Caron, Hugo Touvron, Ishan Misra, Hervé Jégou, Julien Mairal, Piotr Bojanowski, and Armand Joulin. Emerging properties in self-supervised vision transformers. In *Proceedings of the IEEE/CVF international conference on computer vision*, pages 9650–9660, 2021.
- [12] Jean-Bastien Grill, Florian Strub, Florent Altché, Corentin Tallec, Pierre Richemond, Elena Buchatskaya, Carl Doersch, Bernardo Avila Pires, Zhaohan Guo, Mohammad Gheshlaghi Azar, et al. Bootstrap your own latent-a new approach to self-supervised learning. *Advances in neural information processing systems*, 33:21271–21284, 2020.
- [13] Robin Rombach, Andreas Blattmann, Dominik Lorenz, Patrick Esser, and Björn Ommer. High-resolution image synthesis with latent diffusion models. In *Proceedings of the IEEE/CVF conference on computer vision and pattern recognition*, pages 10684–10695, 2022.
- [14] Edward J Hu, Yelong Shen, Phillip Wallis, Zeyuan Allen-Zhu, Yuanzhi Li, Shean Wang, Lu Wang, and Weizhu Chen. Lora: Low-rank adaptation of large language models. *arXiv preprint arXiv:2106.09685*, 2021.

[15] Weiyang Liu, Zeju Qiu, Yao Feng, Yuliang Xiu, Yuxuan Xue, Longhui Yu, Haiwen Feng, Zhen Liu, Juyeon Heo, Songyou Peng, et al. Parameter-efficient orthogonal finetuning via butterfly factorization. *arXiv preprint arXiv:2311.06243*, 2023.

[16] Zeju Qiu, Weiyang Liu, Haiwen Feng, Yuxuan Xue, Yao Feng, Zhen Liu, Dan Zhang, Adrian Weller, and Bernhard Schölkopf. Controlling text-to-image diffusion by orthogonal finetuning. *Advances in Neural Information Processing Systems*, 36:79320–79362, 2023.

[17] Qingru Zhang, Minshuo Chen, Alexander Bukharin, Pengcheng He, Yu Cheng, Weizhu Chen, and Tuo Zhao. Adaptive budget allocation for parameter-efficient fine-tuning. In *The Eleventh International Conference on Learning Representations*, 2023.

[18] Arnav Chavan, Zhuang Liu, Deepak Gupta, Eric Xing, and Zhiqiang Shen. One-for-all: Generalized lora for parameter-efficient fine-tuning. *arXiv preprint arXiv:2306.07967*, 2023.

[19] Vladislav Lalin, Sherin Muckatira, Namrata Shivagunde, and Anna Rumshisky. Relora: High-rank training through low-rank updates. In *Workshop on Advancing Neural Network Training: Computational Efficiency, Scalability, and Resource Optimization (WANT@ NeurIPS 2023)*, 2023.

[20] Chunyuan Li, Heerad Farkhoor, Rosanne Liu, and Jason Yosinski. Measuring the intrinsic dimension of objective landscapes. *arXiv preprint arXiv:1804.08838*, 2018.

[21] Armen Aghajanyan, Luke Zettlemoyer, and Sonal Gupta. Intrinsic dimensionality explains the effectiveness of language model fine-tuning. *arXiv preprint arXiv:2012.13255*, 2020.

[22] Yezhen Cong, Samar Khanna, Chenlin Meng, Patrick Liu, Erik Rozi, Yutong He, Marshall Burke, David Lobell, and Stefano Ermon. Satmae: Pre-training transformers for temporal and multi-spectral satellite imagery. *Advances in Neural Information Processing Systems*, 35:197–211, 2022.

[23] Kumar Ayush, Burak Uzkent, Chenlin Meng, Kumar Tanmay, Marshall Burke, David Lobell, and Stefano Ermon. Geography-aware self-supervised learning. In *Proceedings of the IEEE/CVF International Conference on Computer Vision*, pages 10181–10190, 2021.

[24] Colorado J Reed, Ritwik Gupta, Shufan Li, Sarah Brockman, Christopher Funk, Brian Clipp, Kurt Keutzer, Salvatore Candido, Matt Uyttendaele, and Trevor Darrell. Scale-mae: A scale-aware masked autoencoder for multiscale geospatial representation learning. In *Proceedings of the IEEE/CVF International Conference on Computer Vision*, pages 4088–4099, 2023.

[25] Maofeng Tang, Andrei Cozma, Konstantinos Georgiou, and Hairong Qi. Cross-scale mae: A tale of multiscale exploitation in remote sensing. *Advances in Neural Information Processing Systems*, 36, 2024.

[26] Samar Khanna, Patrick Liu, Linqi Zhou, Chenlin Meng, Robin Rombach, Marshall Burke, David B. Lobell, and Stefano Ermon. Diffusionsat: A generative foundation model for satellite imagery. In *The Twelfth International Conference on Learning Representations*, 2024. URL <https://openreview.net/forum?id=I5webNFDgQ>.

[27] Yukun Zhou, Mark A Chia, Siegfried K Wagner, Murat S Ayhan, Dominic J Williamson, Robbert R Struyven, Timing Liu, Moucheng Xu, Mateo G Lozano, Peter Woodward-Court, et al. A foundation model for generalizable disease detection from retinal images. *Nature*, 622(7981):156–163, 2023.

[28] Alexey Dosovitskiy, Lucas Beyer, Alexander Kolesnikov, Dirk Weissenborn, Xiaohua Zhai, Thomas Unterthiner, Mostafa Dehghani, Matthias Minderer, Georg Heigold, Sylvain Gelly, Jakob Uszkoreit, and Neil Houlsby. An image is worth 16x16 words: Transformers for image recognition at scale. *ICLR*, 2021.

[29] Pang Wei Koh, Shiori Sagawa, Henrik Marklund, Sang Michael Xie, Marvin Zhang, Akshay Balsubramani, Weihua Hu, Michihiro Yasunaga, Richard Lanas Phillips, Irena Gao, et al. Wilds: A benchmark of in-the-wild distribution shifts. In *International conference on machine learning*, pages 5637–5664. PMLR, 2021.

[30] Jun Ma, Yuting He, Feifei Li, Lin Han, Chenyu You, and Bo Wang. Segment anything in medical images. *Nature Communications*, 15(1):654, 2024.

[31] Xin Man, Chenghong Zhang, Jin Feng, Changyu Li, and Jie Shao. W-mae: Pre-trained weather model with masked autoencoder for multi-variable weather forecasting. *arXiv preprint arXiv:2304.08754*, 2023.

[32] Jielu Zhang, Zhongliang Zhou, Gengchen Mai, Lan Mu, Mengxuan Hu, and Sheng Li. Text2seg: Remote sensing image semantic segmentation via text-guided visual foundation models. *arXiv preprint arXiv:2304.10597*, 2023.

[33] George Pu, Anirudh Jain, Jihan Yin, and Russell Kaplan. Empirical analysis of the strengths and weaknesses of peft techniques for llms. *arXiv preprint arXiv:2304.14999*, 2023.

[34] Peeyush Singhal, Rahee Walambe, Sheela Ramanna, and Ketan Kotecha. Domain adaptation: challenges, methods, datasets, and applications. *IEEE access*, 11:6973–7020, 2023.

[35] Arthur Gretton, Karsten M Borgwardt, Malte J Rasch, Bernhard Schölkopf, and Alexander Smola. A kernel two-sample test. *The Journal of Machine Learning Research*, 13(1):723–773, 2012.

[36] Guoliang Kang, Lu Jiang, Yi Yang, and Alexander G Hauptmann. Contrastive adaptation network for unsupervised domain adaptation. In *Proceedings of the IEEE/CVF conference on computer vision and pattern recognition*, pages 4893–4902, 2019.

[37] Baochen Sun, Jiashi Feng, and Kate Saenko. Return of frustratingly easy domain adaptation. In *Proceedings of the AAAI conference on artificial intelligence*, volume 30, 2016.

[38] Yaroslav Ganin, Evgeniya Ustinova, Hana Ajakan, Pascal Germain, Hugo Larochelle, François Laviolette, Mario March, and Victor Lempitsky. Domain-adversarial training of neural networks. *Journal of machine learning research*, 17(59):1–35, 2016.

[39] Haoliang Li, Sinno Jialin Pan, Shiqi Wang, and Alex C Kot. Domain generalization with adversarial feature learning. In *Proceedings of the IEEE conference on computer vision and pattern recognition*, pages 5400–5409, 2018.

[40] Eric Tzeng, Judy Hoffman, Kate Saenko, and Trevor Darrell. Adversarial discriminative domain adaptation. In *Proceedings of the IEEE conference on computer vision and pattern recognition*, pages 7167–7176, 2017.

[41] Weihua Hu, Gang Niu, Issei Sato, and Masashi Sugiyama. Does distributionally robust supervised learning give robust classifiers? In *International Conference on Machine Learning*, pages 2029–2037. PMLR, 2018.

[42] Yonatan Oren, Shiori Sagawa, Tatsunori B Hashimoto, and Percy Liang. Distributionally robust language modeling. *arXiv preprint arXiv:1909.02060*, 2019.

[43] Zhan Tong, Yibing Song, Jue Wang, and Limin Wang. Videomae: Masked autoencoders are data-efficient learners for self-supervised video pre-training. *arXiv preprint arXiv:2203.12602*, 2022.

[44] Roman Bachmann, David Mizrahi, Andrei Atanov, and Amir Zamir. Multimae: Multi-modal multi-task masked autoencoders. *arXiv preprint arXiv:2204.01678*, 2022.

[45] Yatian Pang, Wenxiao Wang, Francis EH Tay, Wei Liu, Yonghong Tian, and Li Yuan. Masked autoencoders for point cloud self-supervised learning. *arXiv preprint arXiv:2203.06604*, 2022.

[46] Sylvain Delattre and Nicolas Fournier. On the kozachenko–leonenko entropy estimator. *Journal of Statistical Planning and Inference*, 185:69–93, 2017.

[47] Timothée Darcet, Maxime Oquab, Julien Mairal, and Piotr Bojanowski. Vision transformers need registers. *arXiv preprint arXiv:2309.16588*, 2023.

[48] Gustav Larsson, Michael Maire, and Gregory Shakhnarovich. Fractalnet: Ultra-deep neural networks without residuals. *arXiv preprint arXiv:1605.07648*, 2016.

[49] Gordon Christie, Neil Fendley, James Wilson, and Ryan Mukherjee. Functional map of the world. In *CVPR*, 2018.

[50] Patrick Helber, Benjamin Bischke, Andreas Dengel, and Damian Borth. Eurosat: A novel dataset and deep learning benchmark for land use and land cover classification. *IEEE Journal of Selected Topics in Applied Earth Observations and Remote Sensing*, 12(7):2217–2226, 2019.

[51] Adam Van Etten, Dave Lindenbaum, and Todd M Bacastow. Spacenet: A remote sensing dataset and challenge series. *arXiv preprint arXiv:1807.01232*, 2018.

[52] Gong Cheng, Junwei Han, and Xiaoqiang Lu. Remote sensing image scene classification: Benchmark and state of the art. *Proceedings of the IEEE*, 105(10):1865–1883, 2017.

[53] Oscar Mañas, Alexandre Lacoste, Xavier Giro-i Nieto, David Vazquez, and Pau Rodriguez. Seasonal contrast: Unsupervised pre-training from uncurated remote sensing data. In *Proceedings of the IEEE/CVF International Conference on Computer Vision*, pages 9414–9423, 2021.

- [54] Peter Bandi, Oscar Geessink, Quirine Manson, Marcory Van Dijk, Maschenka Balkenhol, Meyke Hermsen, Babak Ehteshami Bejnordi, Byungjae Lee, Kyunghyun Paeng, Aoxiao Zhong, et al. From detection of individual metastases to classification of lymph node status at the patient level: the camelyon17 challenge. *IEEE transactions on medical imaging*, 38(2):550–560, 2018.
- [55] Sara Beery, Elijah Cole, and Arvi Gjoka. The iwildcam 2020 competition dataset. *CoRR*, abs/2004.10340, 2020. URL <https://arxiv.org/abs/2004.10340>.
- [56] Jia Deng, Wei Dong, Richard Socher, Li-Jia Li, Kai Li, and Li Fei-Fei. Imagenet: A large-scale hierarchical image database. In *2009 IEEE conference on computer vision and pattern recognition*, pages 248–255. Ieee, 2009.
- [57] Helen Qu and Sang Michael Xie. Connect later: Improving fine-tuning for robustness with targeted augmentations. *arXiv preprint arXiv:2402.03325*, 2024.
- [58] Alexandre Lacoste, Alexandra Luccioni, Victor Schmidt, and Thomas Dandres. Quantifying the carbon emissions of machine learning. *CoRR*, abs/1910.09700, 2019. URL <http://arxiv.org/abs/1910.09700>.

Appendix

We include supplementary material in the following sections.

A Additional Experimental Results

We include further experimental results on downstream datasets as a continuation of section 6.

| Method | PEFT | Top 1 Acc. |
|--------------------|---------|--------------|
| GASSL [23] | Full | 57.63 |
| SatMAE [22] | Full | 71.77 |
| SatMAE [22] | LoRA-r8 | 69.45 |
| MAE [7] | LoRA-r8 | 70.36 |
| DinoV2 [6] | LoRA-r8 | 70.40 |
| D-ExPLoRA- [L]-r32 | LoRA-r8 | 70.40 |

Table 11: NAIP validation set results

Our results (row 6) demonstrate comparable performance, suggesting that for this dataset, domain-specific knowledge may not be highly relevant to successfully solve the task.

B Training Details

In this section, we describe hyperparameters and hardware configurations used for training our models.

B.1 fMoW RGB

Pre-training We use the ViT-Large architecture for all experiments. Since raw image sizes vary, the shorter image size is resized to 224 while preserving aspect ratio, and then a center crop is taken to yield images of size $3 \times 224 \times 224$, representing the channels, height, and width. For D-ExPLoRA configurations, we use the default setting as used in the code provided by [6] (including for the masking probabilities, relative loss weighting, data augmentations and transforms etc.) Similarly, we use the same settings for M-ExPLoRA pre-training as described in [7, 22].

We use a single NVIDIA-RTX 6000 Ada GPU, or 4 NVIDIA-RTX A4000 GPUs for all our experiments, on an academic GPU cluster. For all D-ExPLoRA configurations, we use a batch size of 32, a base learning rate of $1e-3$, no weight decay, and a warmup and decaying cosine learning rate scheduler. We train for 200,000 iterations.

For M-ExPLoRA configurations, we use an effective batch size of 1024 (through gradient accumulation), a base learning rate of $1.5e-4$, no weight decay, and a warmup and decaying cosine scheduler, with a warmup of 1 epoch, and a total training time of 200 epochs.

Fine-tuning We use a base learning rate of $1e-3$, a cosine scheduler with warmup for 1 epoch, and train for 120 epochs. We use an effective batch size of 256, making use of gradient accumulation if the GPU cannot fit the full batch size in memory. We only use the drop-path augmentation, doing away with mixup and cutmix

Our GPU requirements for fine-tuning are the same as in pre-training.

Linear probing We adapt the code provided in [6] for linear probing, with a batch size of 256 and a collection of different learning rates: $[1e-4, 1e-3, 5e-3, 1e-2, 2e-2, 5e-2, 0.1]$. We evaluate both probing on average pooled features as well as on the [CLS] token, and also use output features from just the last block, or the last 4 blocks. All numbers reported represent the best validation set accuracy from the best performing configuration.

B.2 fMoW Sentinel

Pre-training We use the group-channel ViT-L architecture introduced in [22]. We don’t use DinoV2 since there is no such architecture for DinoV2 pre-training. Input images are $13 \times 98 \times 98$, representing 13 multi-spectral bands. We follow the configuration in [22] of dropping bands B1, B9, B10, and use the same grouping strategy. When loading MAE weights to the ViT-L encoder, the patch embeddings do not match and so the patch embedding and group channel encodings are trained from scratch. All other configuration details are the same as for M-ExPLoRA in appendix B.1, except that we use a base learning rate of 4.5e-4 for pre-training and train for 50 epochs (given the larger dataset size) on 4 NVIDIA RTX A4000 GPUs for 80 hours.

B.3 Downstream datasets

Hyperparameter and training configuration details are the same as in appendix B.1 if the images are RGB, and the same as in appendix B.2 if the images have more channels or are temporal.

B.4 Dataset Licenses

The licenses for all datasets are included in the footnotes: fMoW¹, Sentinel-2², EuroSAT³, SpaceNet⁴, Camelyon17⁵, iWildCam⁶

C Environmental Impact

Following [22], we compare the carbon footprint of pre-training using ExPLoRA with domain-specific solutions such as SatMAE. We use the carbon footprint calculator proposed by Lacoste et al. [58]. Our results are in table 12.

| Method | fMoW-RGB | | fMoW-Sentinel | | fMoW-Temporal | |
|---------|-----------|---------------|---------------|--------------|---------------|---------------|
| | GPU hours | kg CO_2 eq. | GPU hours | kg CO_2 eq | GPU hours | kg CO_2 eq. |
| SatMAE | 768 | 109.44 | 576 | 82.08 | 768 | 109.44 |
| ExPLoRA | 96 | 12.44 | 320 | 19.35 | 100 | 12.96 |

Table 12: The estimated carbon footprint of pre-training on these datasets

Since we initialize with pre-trained weights on natural image domains, ExPLoRA is much less environmentally impactful while achieving similar or higher levels of performance. We achieve a 4x-8x reduction in total carbon emitted for each of the large pre-training satellite image datasets considered in table 12.

¹fMoW license: <https://github.com/fMoW/dataset/raw/master/LICENSE>

²Sentinel-2 license: https://scihub.copernicus.eu/twiki/pub/SciHubWebPortal/TermsConditions/Sentinel_Data_Terms_and_Conditions.pdf

³EuroSAT license: <https://creativecommons.org/licenses/by/4.0/>

⁴SpaceNet v1 license: <https://creativecommons.org/licenses/by-sa/4.0/>

⁵Camelyon17 license: <https://creativecommons.org/publicdomain/zero/1.0/>

⁶iWildCam license: <https://cdla.dev/permissive-1-0/>